APPENDIX

PRELIMINARY STUDIES INVOLVING THE RESEARCH

A.1. Stress and strain analysis of abdominal aortic wall: a case of three dimensional geometry simulation

In blood circulation system, the aorta acts as both conduit and an elastic chamber. The elastic of aorta serves to convert the heart's pulsatile flow to steady flow in peripheral vessels. The structural component of vessel wall are altered various conditions such as aging, diabetes and hypertension. That will be a risk factor for arteriosclerosis due to the mechanical properties abnormality through various mechanisms. One of the implications of the structural changes is the change in mechanical properties of the blood vessel. Increased stiffness of large arteries represents an early risk factor for cardiovascular diseases. Therefore, the assessment of aortic mechanical properties is particularly important in understanding the mechanisms of cardiovascular diseases. The major goal of this section is to analyze stress-strain of abdominal aortic wall in a case of three-dimensional geometry simulation.

Mathematical model of abdominal aortic wall: Abdominal aorta geometry in this section was considered three-dimensional thick-walled cylindrical vessel. The abdominal aorta was under statics internal pressure which is from flowing blood pressure acted on inside wall of abdominal aorta. In macroscopic study of aorta, abdominal aorta can be assumed as homogeneous, isotropic and incompressible material. Internal pressure acted on inside wall cause of inflation of abdominal aorta. Experimental parameters from study of Guo and Kassab (2003) were used as initial configuration of this section. As abdominal aorta had no internal pressure, outside diameter of 0.2945 mm, wall thickness of 44.467 micron, elastic modulus of 70 kPa,

poisons ratio of 0.49 were considered. Internal pressures as in mice physiological pressure range of 30, 60, 90, 120 and 150 mmHg were studied.

Theoretical equations: Considering inflation of three-dimensional geometry abdominal aorta as in Figure A.1, plan strain had been suitably used. Plane strain is defined to be a state of strain in which the strain normal to the radial-longitudinal (*r*-*z*) plane and the shear stains $\gamma_{r\theta}$ and $\gamma_{\theta z}$ were assumed to be zero. Assumptions of plane strain are realistic for long vessel (in the *z* direction) with constant cross-sectional area subjected to internal pressure that act only in the radial direction and do not vary in the longitudinal direction. In axisymmatric, the radial displacements developed circumferential strains that induced stresses σ_r, σ_θ, σ_z and γ_{rz}, where *r*, θ and *z* indicated the radial, circumferential and longitudinal directions, respectively. Components of stress related to a cylindrical coordinate system were shown in Figure A.2, using the standard notation $\sigma_{(face)(direction)}$. Triangular torus elements were used to idealize the axisymatric system because they can be used to simulate complex surfaces.

Because of symmetry about the longitudinal axis, the stresses were independent of the θ coordinate (no torsion was considered). Therefore, all derivatives with respected to θ vanished and the displacement component, *v* (tangent to the θ direction), the shear strains, $\gamma_{r\theta}$ and $\gamma_{\theta z}$ and the shear stresses, $\tau_{r\theta}$ and $\tau_{\theta z}$ were all zero.

Strain-displacement relations in cylindrical coordinate system (Boresi and Chong, 2000) were

$$\varepsilon_r = \frac{\partial u}{\partial r} \qquad \varepsilon_\theta = \frac{u}{r}$$
$$\varepsilon_z = \frac{\partial w}{\partial z} \quad \gamma_{rz} = \frac{\partial u}{\partial z} + \frac{\partial w}{\partial r} \tag{A.1}$$

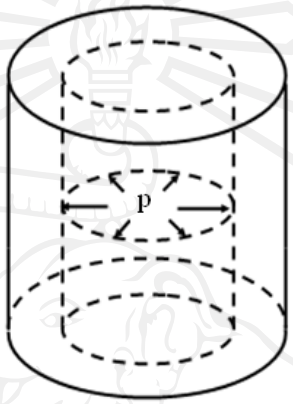

Figure A.1 Thick-walled cylindrical vessel subjected to internal pressure

The isotropic stress-strain relationship, obtained by simplifying the general stress-strain relationships was

$$\begin{Bmatrix} \sigma_r \\ \sigma_z \\ \sigma_\theta \\ \tau_{rz} \end{Bmatrix} = \frac{E}{(1+\nu)(1-2\nu)} \begin{bmatrix} 1-\nu & \nu & \nu & 0 \\ \nu & 1-\nu & \nu & 0 \\ \nu & \nu & 1-\nu & 0 \\ 0 & 0 & 0 & \frac{1-2\nu}{2} \end{bmatrix} \begin{Bmatrix} \varepsilon_r \\ \varepsilon_z \\ \varepsilon_\theta \\ \gamma_{rz} \end{Bmatrix} \tag{A.2}$$

Numerical method: The finite element method is numerical procedure which can model the behavior of structure of vessel. Analytical solutions generally require the solution of ordinary or partial differential equations, which, because of the complication geometry, loading and material properties, are not usually obtainable.

Hence, we need to rely on numerical methods, such as finite element method, for acceptable solutions. Derivation of the strain triangular element stiffness matrix and equations followed these steps.

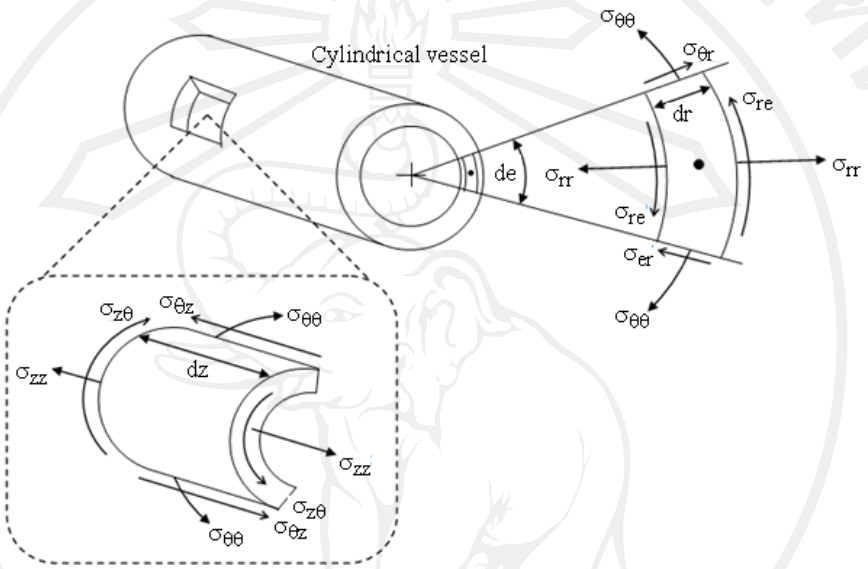

Figure A.2 Components of stress relative to a cylindrical coordinate system

Select element type: Triangular elements as in Figure A.3 were employed because boundaries of irregularly shaped bodies can be closely approximated in this way and because the expressions related to the triangular element were comparatively simple.

Each node had two degrees of freedom, radial and longitudinal displacement. u_i and w_i represent the node i displacement components in the radial and longitudinal direction, respectively. Triangular elements of abdominal aorta and discretized cylinder slice were shown in Figure A.4 and Figure A.5.

Select displacement functions: A linear displacement functions were taken to be

$$u(r,z) = a_1 + a_2 r + a_3 z$$
$$w(r,z) = a_4 + a_5 r + a_6 z \qquad \text{(A.3)}$$

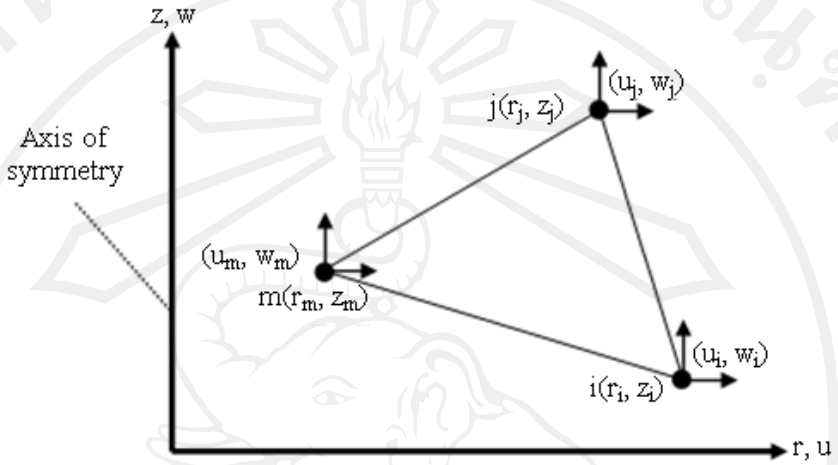

Figure A.3 Triangular element showing degree of freedom

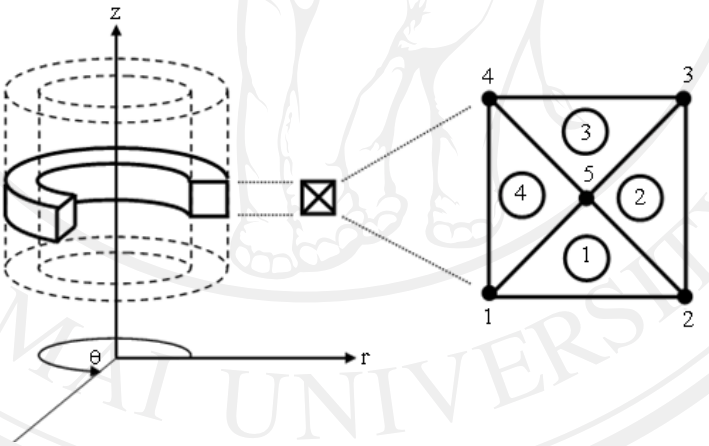

Figure A.4 Triangular elements of abdominal aorta

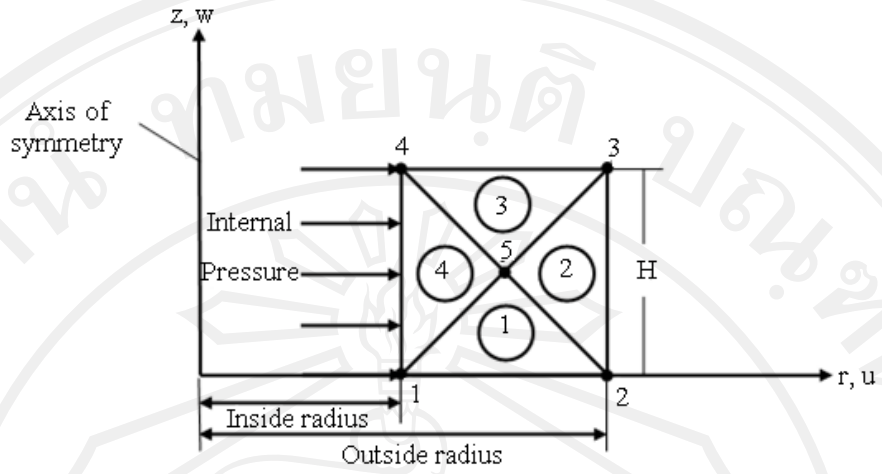

Figure A.5 Discretized cylinder slice

Equation (A.3) were then used to find finite element matrix. Expressing a set of Equation (A.3) in abbreviated matrix form, that was

$$\{\psi\} = [N]\{d\} \tag{A.4}$$

where

$\{\psi\}$ = The displacement function

$[N]$ = The shape functions represented the shape of $\{\psi\}$

$\{d\}$ = Displacement matrix

Nodal displacements can be calculated by Equation (A.4)

Define the strain-displacement and stress-strain relationships: Equation (A.1) were used and then rewritten in finite element matrix form as

$$\{\varepsilon\} = [B]\{d\} \tag{A.5}$$

where, [B] is a function of the radial and longitudinal coordinates. Equation (A.2) was used and then rewritten in finite element matrix form as

$$\{\sigma\} = [D][B]\{d\} \tag{A.6}$$

where, [D] is given by the first matrix on the right side of Equation (A.2). Strains of elements obtained from Equation (A.5) were used to calculate stresses of elements.

Derive the element stiffness matrix and equations: Using principle of minimum potential energy, the equations can be generated for strain triangular element. The equation of system obtained by principle of minimum potential energy was

$$\iiint_V [B]^T[D][B]dV\{d\} = \{f\} \tag{A.7}$$

It can be seen that the stiffness matrix was

$$[k] = \iiint_v [B]^T[D][B]dV \tag{A.8}$$

or

$$\left[k\right] = 2\pi\iint_A \left[B\right]^T\left[D\right]\left[B\right]rdrdz \tag{A.9}$$

Method which was used to evaluate Equation (A.9) was from [B] evaluation by a centroidal point of element.

Surface force from internal pressure can be found by:

$$\{f\} = \iint_S [N_s]^T \{T\} dS \qquad (A.10)$$

Assemble the element equations: The element equations assembly was in order to obtain the global equations and introduce boundary conditions.

Solve for the nodal displacements: Nodal displacements were used in Equation (A.5) to calculate strains of elements.

Solve for the elements forces (stresses): Strains of elements obtained by using Equation (A.5) were used to calculate stresses of elements.

Results were shown in Figure A.6 through Figure A.11. To verify present simulation, the simulation results were compared with the experimental data from Guo and Kasseb (2003).

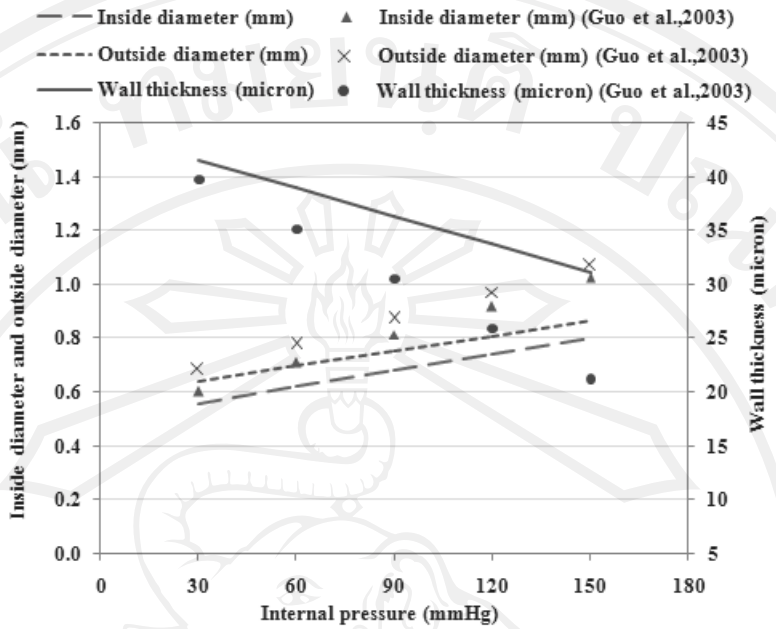

Figure A.6 Effect of internal pressure on inside diameter, outside diameter and wall thickness

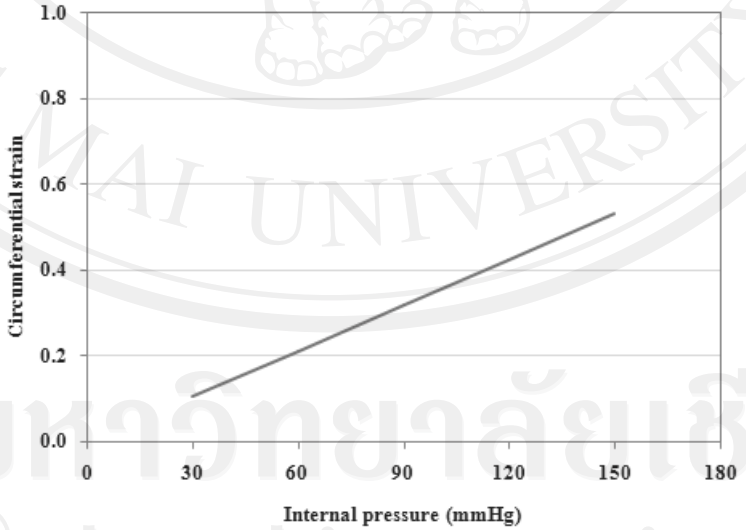

Figure A.7 Effect of internal pressure on circumferential strain

Effect of internal pressure on inside diameter, outside diameter and wall thickness, effect of internal pressure on circumferential strain, effect of internal pressure on lumen cross-sectional area and effect of internal pressure on radial stress, longitudinal stress and circumferential stress were shown in Figure A.6, A.7, A.8 and A.9, respectively.

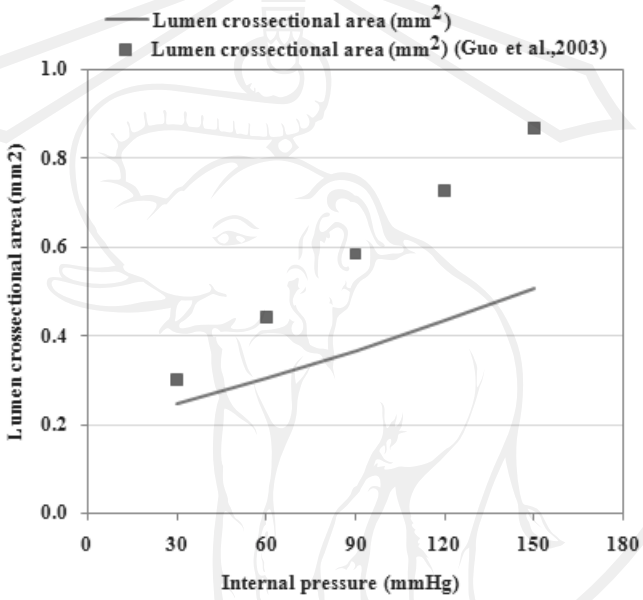

Figure A.8 Effect of internal pressure on lumen cross-sectional area

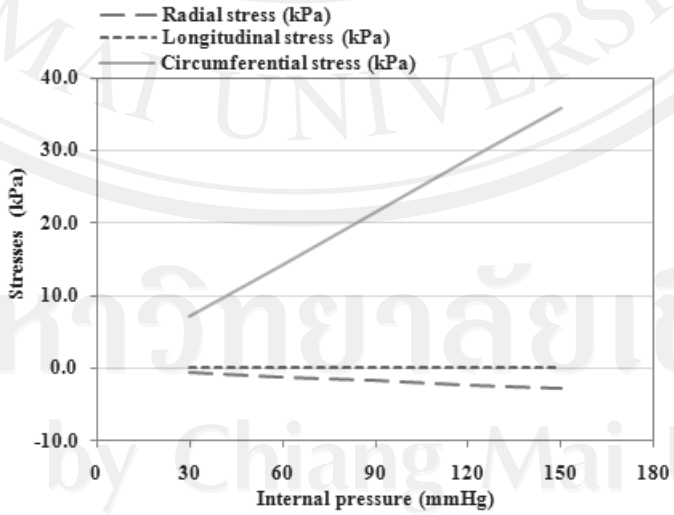

Figure A.9 Effect of internal pressure on radial stress, longitudinal stress and circumferential stress

Also, it can be seen circumferential stress-strain relationship in Figure A.10. Moreover, radial, longitudinal and circumferential stress distributions across wall thickness at mean pressure of 96.4 mmHg of mice was shown in Figure A.11.

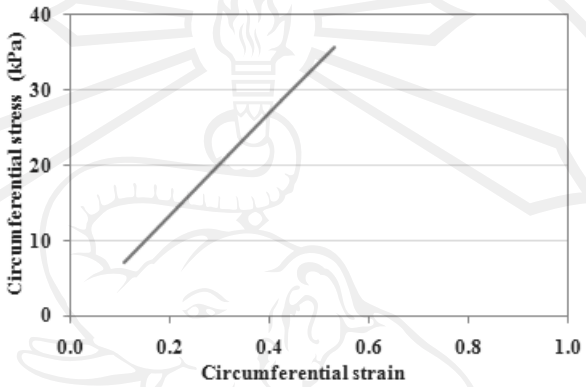

Figure A.10 Circumferential stress-strain relationship

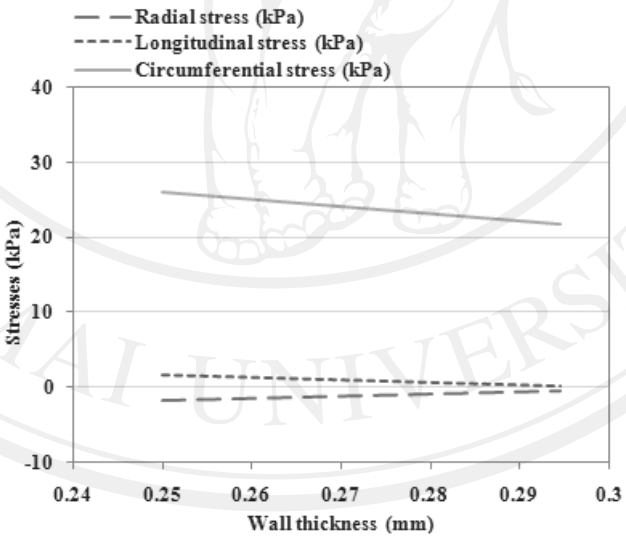

Figure A.11 Radial, longitudinal and circumferential stress distributions across wall thickness at mean pressure of 96.4 mmHg of mice

From the results, it was found that effect of internal pressure on inside diameter, outside diameter as Figure A.6 had the same trend to results of Guo and Kasseb (2003). Although present results had a little difference with results of Guo and Kasseb (2003) but these diameters had been the same order of magnitude. These show that this simulation was shown good agreement. From this result, it can be seen that, when internal pressure increased, both of inside diameter and outside diameter linearly increased. But, increasing of inside diameter with internal pressure was greater than increasing of outside diameter. This difference of increasing of inside diameter and outside diameter resulted in wall thickness (wall thickness was computed as the difference between the outside and inside radius of vessel at different pressure) reduction linearly with internal pressure as shown in Figure A.6. Again, in this trend of wall thickness reduction of present result, it was also seen in result of Guo and Kasseb (2003) as well.

Moreover, the variation of the average circumferential strains with pressure was computed. As internal pressure resulting in increasing of both diameters, it also resulted in linearly increasing of circumferential strain of abdominal wall as shown in Figure A.7.

The variation of lumen cross-sectional area with pressure of abdominal aorta was found to be linear as shown in Figure A.8. Present result of effect of internal pressure on lumen cross-sectional area had the same trend to result of Guo and Kasseb (2003) but there had more difference because lumen cross-sectional area of abdominal aorta increased by square of internal diameter at that internal pressure.

Hence, it can be stated that the linearity between pressure and various metric parameters (diameter, wall thickness, lumen cross-sectional area) in a large range of

pressure (30-150 mmHg) was remarkable. The wall thickness decreased, whereas the diameter, lumen cross-sectional area increased.

The compliance can be expressed in terms of cross-section area. The result of the mouse cross-sectional area compliance was shown as slope of lumen cross-sectional area and internal pressure in Figure A.8.

The variations of radial stress, longitudinal stress and circumferential stress of abdominal aorta with internal pressure are shown in Figure A.9. Similarly, the stresses varied linearly with pressure in the pressure range of 30-150 mmHg. In Figure A.9, it can be seen that the magnitude of radial stress, longitudinal stress and circumferential stress increased with increasing internal pressure. And, from Figure A.11, these values were largest at the inside surface. The radial stress was of course compressive and varies from a value equal to the negative of the internal pressure at the inside to zero at the outside.

Relationship of circumferential stress-strain of abdominal aorta was shown in Figure A.10. This figure was shown that stress in circumferential direction linearly increased with strain in circumferential. Slope of this stress-strain was elasticity of abdominal aorta of 70 kPa which was a constant as assumed previously.

Stress-strain analysis of abdominal aortic wall in a case of 3D geometry simulation had been simulated using numerical model. This model was verified with experimental data from Guo and Kassab (2003). Good agreement had been obtained. The wall thickness decreased, whereas the diameter, lumen cross-sectional area increased with internal pressures. The magnitude of radial stress, longitudinal stress and circumferential stress increased with increasing internal pressure and values were largest at the inside surface. The radial stress was of course compressive and varied

from a value equal to the negative of the internal pressure at the inside to zero at the outside.

In summary, this section analyzed stress-strain of abdominal aortic wall in three dimensional geometry simulation. Abdominal aorta is a portion of the aorta vessel in the abdomen which many cardiovascular diseases often occur. Abdominal aortic wall was considered as one layers-three dimensional cylindrical geometry and homogeneous, incompressible and anisotropic material. Deformation of aortic wall was elastic deformation. Numerical method was used in our simulation. The abdominal aorta was under luminal loading of pressure in physiological pressure range of mice. Experimental parameters from previous study were used as initial configuration of this section. To verify present simulation, the simulation results were compared with the experimental data from previous study. From the simulation, the wall thickness decreased, whereas the diameter, lumen cross-sectional area increased with internal pressures. The magnitude of radial stress, longitudinal stress and circumferential stress increased with increasing internal pressure and values were largest at the inside surface. The radial stress was obviously compressive and varied from a value equal to the negative of the internal pressure at the inside to zero at the outside. Stress-strain analysis of abdominal aortic wall in a case of three dimensional geometry simulation can be simulated using numerical model. This model had been verified with experimental data from previous study. Good agreement was obtained. Mathematical model which considering aortic wall by using finite element method could be beneficially used as addition data for medical diagnosis.

A.2 A comparative study of stress and strain analysis of murine abdominal aortic wall based on ultrasound data: cases of thin wall and thick wall

The major goal of this section was to analyze stress and strain of abdominal aortic wall based on ultrasound data and to interpret by a comparative study of mechanical simulations of thin walled and thick walled abdominal aortic vessel.

A murine abdominal aorta was canulated using an ultraminiature pressure catheter (SciSense, London, ON, Canada) through the mouse carotid artery and introduced into the abdominal aortic region. The ECG was acquired using the electrode leads available on the heating mouse platform (THM100, Indus, Instruments, Houston, TX). Both luminal pressure and ECG signals were acquired by using a two channel 14-bit waveform digitizer (CompuScope 14200, Gage Applied Technologies Inc., Lachine, QC, Canada) at sampling frequency of 10 kHz. A 30-MHz ultrasound probe (RMV-707B, VisualSonics Inc., Toronto,ON, Canada) was placed on the murine abdomen. A longitudinal view of the abdominal aorta was used so as to align the radial direction of the aorta with the axial direction of the ultrasound beams. Following data acquisition, the acquired RF signals were gated between two consecutive R-waves to reconstruct the image sequence for a complete cardiac cycle at the extremely high frame rate of 8 kHz. Along an abdominal aortic length of 12 mm, the incremental axial displacements, parallel to the radial direction of the abdominal aorta, were estimated off-line using a one dimensional normalized cross-correlation technique on the acquired RF signals.

A single luminal pressure profile in a specific aortic region was assumed to represent the pressure over the entire scanned abdominal region corresponding to the diameter variation in every longitudinal location of the abdominal aorta. The inside

and outside aortic diameters and abdominal aortic wall regions were clearly obtained through manual tracing on the B-mode image. The radial incremental displacements of the inside and outside walls were then calculated. These were accumulated to obtain the wall diameter variation over one cardiac cycle. The luminal pressure and aortic wall diameter variations were matched using the corresponding ECG. Since the aortic wall behavior was assumed to be elastic, the phase shift between the pressure and diameter variations, resulting from viscoelastic behavior, was ignored. Hence, the maximum and minimum peaks of the luminal pressure and diameter variations were aligned. The aortic dilation from the minimum to maximum diameter peak was measured in order to interpret the aortic dilation behavior.

Two mechanical simulations were used to study behavior the abdominal aortic vessel. One was mechanical simulation for thin walled abdominal aortic vessel and the other one was mechanical simulation for thick walled abdominal aortic vessel.

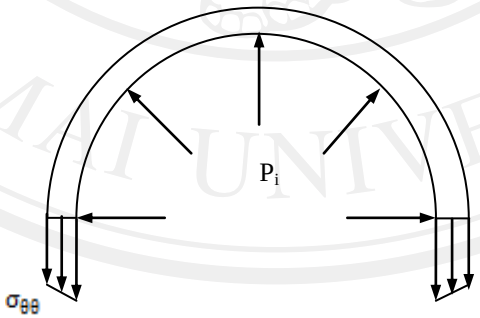

Figure A.12 The radial distribution of the circumferential stress $\sigma_{\theta\theta}$ in a thin walled portion of cylinder aortic vessel under an luminal pressure P_i. The circumferential stress $\sigma_{\theta\theta}$ was non-uniform but nearly constant stresses.

Starting with the mechanical simulation for thin walled abdominal aortic vessel, the vessel was idealized as cylindrical and thin walled tube which it is so reasonable to assume the stress is approximately uniform across the thickness. To obtain circumferential stress for pressurization of thin walled vessel, the cylindrical abdominal aortic vessel should be considered in a half cut as Figure A.12.

A force balance in vertical direction was required. The net vertical force was obtained from summation of all uniform luminal pressures P_i acting at each point on inside surface of the vessel multiplied by respective differential area *dA*. This vertical force was balanced to summation of circumferential stresses $\sigma_{\theta\theta}$ at each point multiplied by respective differential area *dA*. Hence, force balance in vertical direction can be written as

$$\sum F_v=0;\ \int P_v\, dA-2\int \sigma_{\theta\theta}\, dA=0. \qquad \text{(A.11)}$$

The vertical pressure P_v can be written in term of the luminal pressure as $P_v=P_i\sin\theta$ which acting over the differential area of $r_i d\theta dz$. And, the circumferential stresses $\sigma_{\theta\theta}$ acted on differential area of drdz, as shown by free body diagram in Figure A.13.

Therefore, the equation for determining the circumferential (Cauchy) stress yielded

$$\sigma_{\theta\theta}=\frac{P_i r_i}{h}. \qquad \text{(A.12)}$$

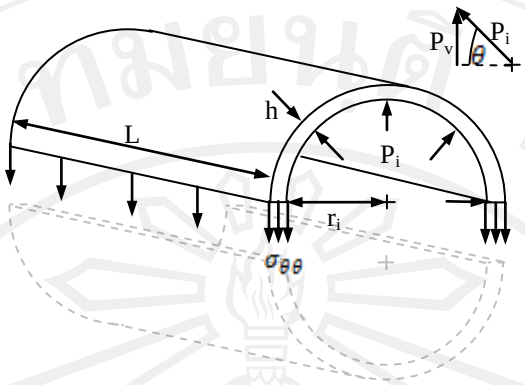

Figure A.13 A half cut of thin cylindrical abdominal aortic vessel subjected by an luminal pressure where L, r_i and h denoted as length of vessel, inside radius and thickness, respectively.

By boundary conditions, to obtain radial stress σ_{rr}, the radial stress σ_{rr} equaled to $-P_i$ at inside surface and the radial stress σ_{rr} equaled to $-P_o$ of zero at outside surface. The radial stresses within the wall of thin walled vessel was simply assumed as

$$\sigma_{rr} = \frac{(-P_i)+(-P_o)}{2} \cong \frac{-P_i}{2} . \qquad \text{(A.13)}$$

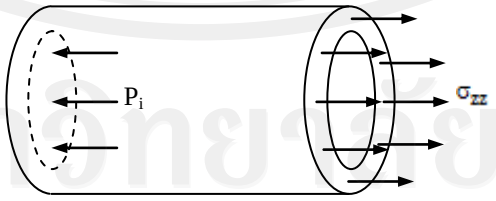

Figure A.14 Free body diagram of cylinder vessel for consideration of axial force balance

To obtain axial stress, the vessel was considered as the ends of the vessel were closed. Thus, the luminal pressure P_i subjected normal into all surfaces which also provided a net axial load as shown in Figure A.14.

Summation of forces was performed again in the axial direction. The net axial force was obtained from summation of all uniform luminal pressures P_i acting at each point on inside surface of the vessel multiplied by respective differential area *dA.* This axial force was balanced to summation of axial stresses σ_{zz} at each point multiplied by respective differential area *dA.* Hence, force balance in axial direction can be written as

$$\sum F_z=0;\ \int P_i\, dA-\int \sigma_{zz}\, dA=0 \qquad \text{(A.14)}$$

The luminal pressure P_i and the axial stresses σ_{zz} , both were acted over the differential area of $r_i d\theta dr$. Therefore, by assuming the term h^2 was relative small to $2r_i h$, the equation for determining the axial stress yielded

$$\sigma_{zz}=\frac{P_i r_i}{2h}. \qquad \text{(A.15)}$$

Since, the circumference of vessel was proportional to its radius, thus, the circumferential strain can be written as

$$\varepsilon_{\theta\theta}=\frac{r_{mean}-R_{mean}}{R_{mean}} \qquad \text{(A.16)}$$

where mean radius r_{mean} denoted as average of inside and outside radius in current configuration and R_{mean} denoted as average of inside and outside radius in reference configuration defined as the minimum vessel radius over a cardiac cycle.

In the mechanical simulation for thick walled abdominal aortic vessel, pressurization of cylinder exhibited linear elastic, homogeneous and isotropic. Complete axisymmetry was assumed. Since, vessel was subjected by uniform pressure and axial load applied through centroid, thus, possible stresses in Figure A.15 were only in normal directions which vary with radial location. The cylindrical equilibrium equation in absence of body force can be written as

$$\frac{d\sigma_{rr}}{dr} + \frac{1}{r}\left(\sigma_{rr}-\sigma_{\theta\theta}\right)=0\,. \tag{A.17}$$

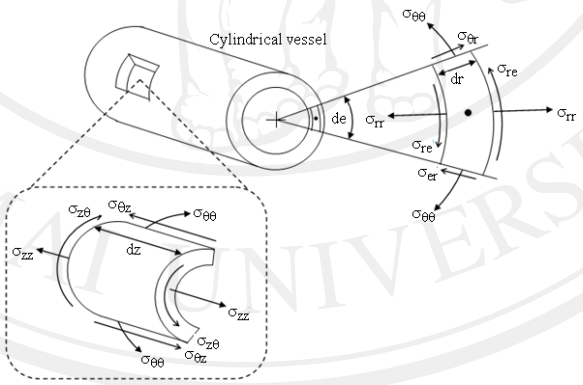

Figure A.15 Components of stress relative to a cylindrical coordinate system

Normal strains in all three directions were

$$\varepsilon_{rr}=\frac{\partial u_r}{r},\ \varepsilon_{\theta\theta}=\frac{u_r}{r},\ \varepsilon_{rr}=\frac{\partial u_z}{\partial z} \tag{A.18}$$

with compatibility equation as

$$\frac{d}{dr}(r\varepsilon_{\theta\theta})=\varepsilon_{rr}\,. \tag{A.19}$$

By boundary conditions, to obtain radial stress σ_{rr}, the radial stress σ_{rr} equaled to $-P_i$ at inside surface and the radial stress σ_{rr} equaled to $-P_o$ of zero at outside surface. Thus, the radial stresses σ_{rr} within the wall of thick walled vessel can be written as

$$\sigma_{rr}=\frac{P_i r_i^2 - P_o r_0^2}{r_o^2 - r_i^2} - \frac{(P_i - P_o) r_i^2 r_o^2}{(r_0^2 - r_i^2) r^2} \tag{A.20}$$

where subscripts i and o denoted as inside and outside, respectively. Then, the circumferential stress $\sigma_{\theta\theta}$ was obtained as

$$\sigma_{\theta\theta}=\frac{P_i r_i^2 - P_o r_0^2}{r_o^2 - r_i^2} + \frac{(P_i - P_o) r_i^2 r_o^2}{(r_0^2 - r_i^2) r^2}\,. \tag{A.21}$$

The stresses had already related to pressure and radius. To maintain inflated vessel at fixed length, the axial stress σ_{zz} was required that given by

$$\sigma_{zz}=\frac{2\upsilon P_i r_i^2}{r_o^2 - r_i^2} \tag{A.22}$$

Material property υ was involved which is in contrast to in thin walled vascular case and the vascular wall was assumed to be incompressible which υ of 0.49 was used. Luminal pressures of 40, 50, 60, 70, 80 and 90 mmHg were used in this section.

Stress and strain of abdominal aortic wall were analyzed based on ultrasound data and then interpreted by a comparative study of mechanical simulations of thin walled and thick walled abdominal aortic vessel.

Results were shown in Figure A.16 through Figure A.19. Two mechanical simulation analyses of thin walled and thick wall abdominal aortic vessel were shown.

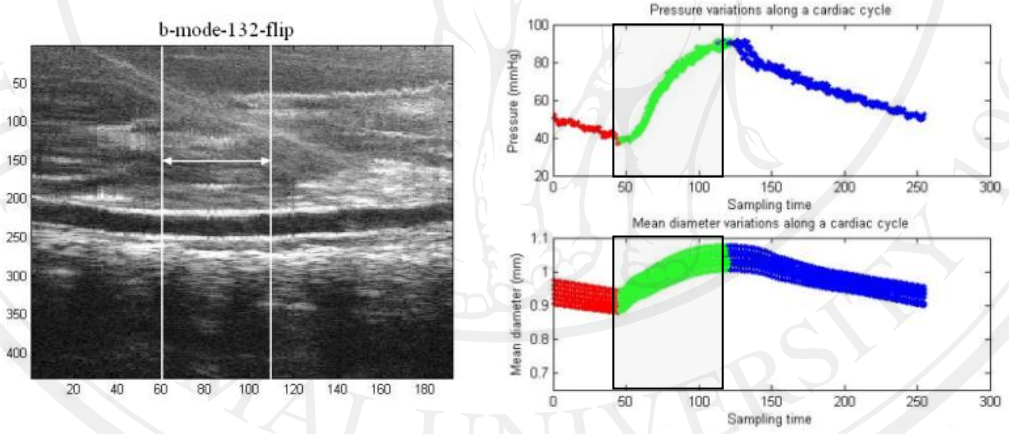

(A) (B)

Figure A.16 The B-mode image of the mouse abdominal aortic vessel (A). Pressure (mmHg) variation along a cardiac cycle (B upper) and mean diameter (mm) variation along a cardiac cycle (B lower) were shown in (B)

The B-mode image of the mouse abdominal aortic vessel in Figure A.16(A) was then traced. Reference inside diameter, reference outside diameter, incremental displacement, inside diameter, outside diameter and wall thickness of 23 positions

along longitudinal length of abdominal aortic vessel in the range as shown by white arrow in Figure A.16(A) were obtain. The maximum and minimum peaks of the luminal pressure and diameter variations were aligned and then aortic dilation range as can be seen in Figure A.16(B) which colored in gray area was attended.

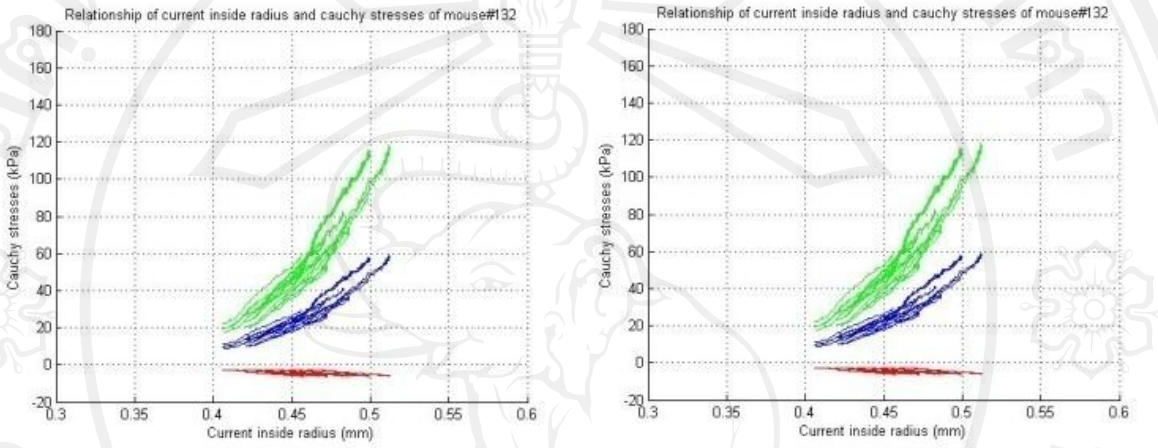

(A) (B)

Figure A.17 Relationship of current radius (mm) and Cauchy stresses (kPa) obtained from mechanical simulation analyses of thin walled (A) and thick wall (B) abdominal aortic vessel. Cauchy stresses of all three normal stresses which were radial stress, circumferential stress and axial stress was in red, green and blue line.

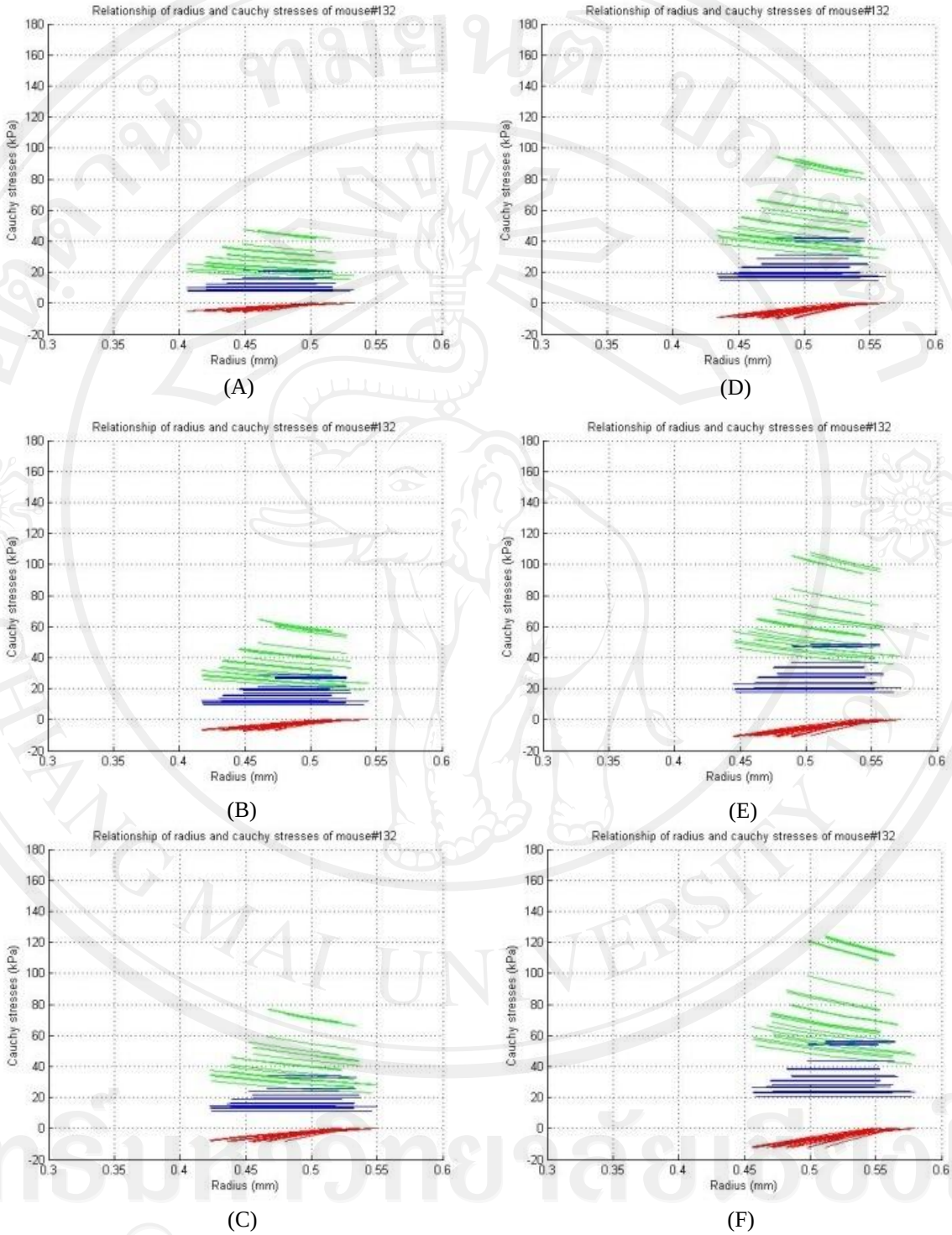

Figure A.18 Relationship of radius (mm) and Cauchy stresses (kPa) obtained from mechanical simulation analysis of thick walled abdominal aortic vessel and subjected by luminal pressure of 40(A), 50(B), 60(C), 70(D), 80(E) and 90(F) mmHg.

Relationship of current radius and Cauchy stresses obtained from mechanical simulation of thin walled abdominal aortic vessel can be shown in Figure A.17(A) and relationship of current radius and Cauchy stresses obtained from mechanical simulation of thick walled abdominal aortic vessel at mid wall can be shown in Figure A.17(B). Cauchy stresses plotted in Figure A.17 were radial stress, circumferential stress and axial stress.

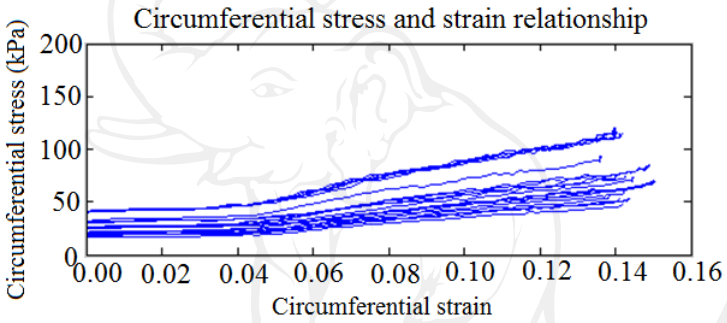

Figure A.19 Circumferential stress (kPa) and strain relationship

In mechanical simulation of thick walled abdominal aortic vessel, luminal pressures subjected to the vessel were considered from 40 mmHg, which each increased for 10 mmHg, until reached to 90 mmHg. Relationship of radius and Cauchy stresses across wall thickness can be determined as shown in Figure A.18(A)-(F). Finally, circumferential stress and circumferential strain relationship can be obtained as in Figure A.19.

In the following, we first discuss experimental considerations and then discuss the mechanical simulation analyses of thin walled and thick wall abdominal aortic vessel. Ultrasound imaging allowed us to obtain reliable importance parameters. Tracing B-mode image of the mouse abdominal aortic vessel provided

reference inside diameter, reference outside diameter, incremental displacement, inside diameter, outside diameter and then wall thickness of 23 positions along longitudinal length of abdominal aortic vessel in the range as shown by white arrow can be easily determined. Performing alignment the maximum and minimum peaks of the luminal pressure and diameter variations as can be seen in gray area of Figure A.16(A) allowed us to attend in aortic dilation range. From the result of the mechanical simulation analysis of thin walled abdominal aortic vessel, the stresses of radial, circumferential and axial stress varied with luminal pressure in the range of 40-90mmHg as shown in Figure A.17(A), it can be observed that increasing diameter resulted from subjected by increasing luminal pressure from 40 to 90 mmHg resulted in increasing magnitude of the stresses of radial, circumferential and axial stress. Moreover, the stresses varied nearly linear with current inside radius. The radial stress was compressive which in contrast to the circumferential and axial stress. Thin walled abdominal aortic vessel consideration yielded the average value of the stress regardless of the material properties or the thickness.

On the other hand, from the result of the mechanical simulation analysis of thick walled abdominal aortic vessel, it can be observed from Figure A.18 that the magnitudes of the stresses of radial, circumferential and axial stress were largest at the inside wall. Radial stress varied from a value equal to the negative of the internal pressure at the inside wall to external pressure at the outside wall by increases monotonically from $-P_i$ to $-P_o$ which also seen again that radial stress was always compressive and circumferential stress decreases monotonically from maximum value at inside wall. Radial stress value was smaller in comparison to that of circumferential stress. From Figure A.18 in which considered stresses across wall thickness, the

thinnest walled of local position vessel had the highest stress which can be implied that it had less material to resist the same load. The axial stress is uniform even though the radial and circumferential components were not. Both of the mechanical simulations of thin walled and thick wall abdominal aortic vessel gained useful information of stress and strain. Relationship between the stresses and the luminal pressures and the radius which represented of the aortic vessel geometry can be found without specifying the material in thin walled vessel simulation while the material properties of linear elastic, homogeneous and isotropy were assumed in thick walled vessel simulation. The results of thin walled vessel simulation were mostly used because it was allowed analysis of boundary value problem that provided means of material behavior by their stresses can be represented well by the average value. This interpret can be assured by in comparison the mechanical simulation using thick walled vessel at mid wall (Figure A.17(B)) to the mechanical simulation using thin walled vessel (Figure A.17(A)) that the result was seen to equal exactly the thin walled vessel. Beside, differential equations were solved to find the distribution of stress in the thick walled vessel, whereas simple force balance equations are solved to find the uniform (average) stresses in the thin walled vessel. The relationship between circumferential stress and circumferential strain can be determined by the mechanical simulation of thin walled abdominal aortic vessel and also shown as in Figure A.19. It was seen that the relationship between them was not proportional over the wide range of internal pressure which may because of its structure consisted of different composition of each layer such as the major cellular of endothelial, smooth muscle and matrix of elastin and collagen. More material properties of vessel were required

further studies in which more approach to realistic abdominal aortic vessel to obtain useful information data for medical diagnosis.

Stress and strain analysis of abdominal aortic wall has been successfully simulated by using useful data of ultrasound technique. Experimental considerations and the mechanical simulation analyses of thin walled and thick wall abdominal aortic vessel were discussed. Mechanical simulation which consider stress and strain aortic wall could be beneficially used as additional data for medical diagnosis.

In summary, the major goal of this section was to analyze stress and strain of abdominal aortic wall based on ultrasound data and to interpret by a comparative study of mechanical simulations of thin walled and thick walled abdominal aortic vessel. Luminal pressure variation was measured using ultra-miniature pressure catheter. Wall geometry and motion of abdominal aorta of mice were detected by using ultrasound imaging technique. Cross-correlation technique was used to effectively provide displacement of the aortic wall. The displacement and luminal pressure variation then were used in mechanical simulation to determine Cauchy stress and strain in three major directions of circumferential, radial and longitudinal directions of abdominal aortic wall. Abdominal aortic wall was considered under physiological loads of pressurization and extension and was assumed as perfectly cylindrical tube and homogeneous, incompressible, isotropic material. Deformation of the aortic wall was elastic deformation. Two mechanical simulation analyses of thin-walled and thick-wall abdominal aortic vessel were compared and interpreted. It was found in both of two mechanical simulation analyses that, three Cauchy stresses and strains distributions along radius were obtained. It can be seen in a mechanical simulation of thin walled aortic vessel that average stresses located at middle wall can

be obtained. The magnitude of circumferential, radial and longitudinal stresses increased with increasing luminal pressure. The radial stress was obviously compressive. Also, it can be seen the magnitude variations of the stresses and the compressive radial stress in a mechanical simulation of thick-walled aortic vessel. Moreover, the magnitude of these stresses were largest at the inside surface and the radial stress varied from a value equal to the negative of the luminal pressure at the inside surface to zero at the outside surface. It was meant that consideration in three directions obtains more understanding. Stress and strain analysis of abdominal aortic wall can be simulated by using useful data of ultrasound technique. Mechanical simulation which consider stress and strain aortic wall could be beneficially used as additional data for medical diagnosis.

CURRICULUM VITAE

Name	Miss Pannathai Khamdaengyodtai
Date of birth	January 22nd, 1985
Educations	***Doctor of Philosophy Program*** (Mechanical Engineering), GPA 4.00/4.00, Chiang Mai University THAILAND ***Bachelor of Engineering*** (Mechanical Engineering), 2nd honors, Chiang Mai University, THAILAND
Research interests	Cardiovascular system, vascular biomechanics, material mechanics, nonlinear elasticity, numerical method, and thermo-fluid
Academic experience	***Visiting scholar***, 2011-2012, Mechanical Engineering, Bourns College of Engineering, University of California, Riverside, USA ***Teaching Assistant***, 2009-2010, Chiang Mai University, Department of Mechanical Engineering, Chiang Mai, THAILAND, Course: Heat Pipe Technology.
Journal publications	1. P. Khamdaengyodtai, T. Khamdaeng, P. Sakulcahng-satjatai, N. Kammuang-lue and P. Terdtoon, "Stresses and Strains Distributions in Three-Dimension Three-Layer Abdominal Aortic Wall Based on *in vivo* Ultrasound Imaging", *Journal of Science and Technology Mahasarakham University*, 31(5), 2012.

2. P. Khamdaengyodtai, P. Sakulchangsatjatai and P. Terdtoon, "Stress-Strain Analysis of Abdominal aortic wall: A Case of 3D Geometry Simulation", *Energy Research Journal*, 1: 165-170, 2010. ***DOI:*** 10.3844/ejsp.2010.165.170

Conference proceeding

P. Khamdaengyodtai, P. Terdtoon and P. Sakulchangsatjatai, "A Comparative Study of Stress and Strain Analysis of Murine Abdominal Aortic Wall Based on Ultrasound Data: Cases of Thin Wall and Thick Wall"**,** *The second International Conference on Science, Technology and Innovation for Sustainable Well-Being***,** Quang Binh University, Vietnam, August 13-14, 2010.

Scholarship

The Thailand Research Fund through the Royal Golden Jubilee Ph.D.Program (PHD/0181/2549, 1.M.CM/49/A.1), 2007-2012

Awards

1. 2nd honor in Bachelor of Engineering (Mechanical Engineering), 2007

2. 2 bronze coin certificates of high score mechanical engineering student, 2005-2006